Journal of
Materials Chemistry A

ROYAL SOCIETY
OF CHEMISTRY

PAPER

View Article Online
View Journal | View Issue

Cite this: *J. Mater. Chem. A*, 2021, **9**, 11427

Molecular engineered palladium single atom catalysts with an M-C_1N_3 subunit for Suzuki coupling†

Jia Liu,‡[ab] Zhongxin Chen,‡[a] Cuibo Liu,‡[ac] Bao Zhang,[b] Yonghua Du,[d] Chen-Fei Liu,[a] Lu Ma,[d] Shibo Xi,[e] Runlai Li,[a] Xiaoxu Zhao,[a] Jingting Song,[af] Xin Zhi Sui,[b] Wei Yu,[a] Ling Miao,*[b] Jianjun Jiang,[b] Ming Joo Koh*[a] and Kian Ping Loh*[a]

Received 1st January 2021
Accepted 16th April 2021

DOI: 10.1039/d1ta00012h

rsc.li/materials-a

Single atom catalysis has emerged as a powerful technique for catalysis due to its outstanding performance and atom economy. Controlling the hybridization of the atom with its environment is crucial in determining the selectivity and/or yield of the reaction. However, the single atom environment is usually ill-defined and hard to predict because the pyrolysis process used in preparing SACs damages the original status of the precursors in the catalyst preparation. A molecular engineering approach to synthesize single atom catalysts (SACs) on a heterogeneous template provides a strategy to make SACs with a highly uniform coordinating environment. Herein, we report the preparation of a molecular engineered Pd single atom catalyst with a pre-defined M-N_3C_1 coordination (Pd-N_3C_1-SAC) using a structure-rigid Pd-N_3C_1 porphyrin as the precursor, which shows more efficient Suzuki coupling compared with the SAC with Pd-N_4 coordination. The origin of the high activity of the Pd-N_3C_1-SAC is revealed through density functional theory calculations, where a lower reaction barrier for the rate-determining oxidative addition is identified.

Introduction

Industrial production of commodity and fine chemicals requires a highly selective catalytic process owing to the high demands for purity and cost-effectiveness.[1] Single atom catalysis has witnessed rapid developments in the last decade owing to atom economy, ultrahigh turnover frequency and unique selectivity.[1–3] Unfortunately, applications of SACs were largely limited to gas phase reactions or electrocatalysis due to the lack of sufficient activation of reactants by single metal sites under liquid phase conditions.[4,5] Considerable efforts have been devoted to address this by improving the catalyst design, where successful examples in SAC-catalysed, selective hydrogenation and oxidation were reported.[4,5] For instance, we have recently disclosed the first SAC-catalysed preparation of pharmaceuticals (Lonidamine)[6] and late-functionalization (Tamiflu®)[7] through selective hydrogenation of α-diazoesters to *E*-hydrazones and selective oxidation of sulfides to sulfoxides and sulfones, respectively.

Among various strategies to assemble complex molecules, carbon–carbon bond formation by palladium-catalysed Suzuki coupling remains one of the most important reactions owing to its wide applications across the industry.[8–11] The uniqueness of Pd_1 SACs in cross-coupling has recently been demonstrated by Pérez-Ramírez *et al.*,[8] where Pd_1 SACs exhibited an excellent turnover frequency in a continuous-flow setup. Progress on Suzuki, Ullmann, Sonogashira and Heck couplings had also been reported using heterogeneous SACs,[9–14] however, efficiencies were generally poorer than homogeneous variants possibly due to the lack of a dynamic catalytic cycle involving Pd^0/Pd^{2+} states for the oxidative addition-reductive elimination pathway.[15–21] Regulation of the catalytic center by pyrolysis is difficult when using unstable Pd precursors.[22–24] This calls for a molecularly precise approach to control the catalytic centre, together with morphological engineering to maximize the exposure of active sites.

---

[a] *Department of Chemistry, National University of Singapore, 3 Science Drive 3, Singapore 117543, Singapore. E-mail: chmkmj@nus.edu.sg, chmlohkp@nus.edu.sg*

[b] *School of Optical and Electronic Information, Huazhong University of Science and Technology, Wuhan 430074, PR China. E-mail: miaoling@mail.hust.edu.cn*

[c] *Department of Chemistry, Institute of Molecular Plus, School of Science, Tianjin University, Tianjin, 300072, China*

[d] *National Synchrotron Light Source II, Brookhaven National Lab, Upton, New York 11973, USA*

[e] *Institute of Chemical and Engineering Sciences, Agency for Science, Technology and Research, 1 Pesek Road, Jurong Island, Singapore 627833, Singapore*

[f] *Joint School of NUS and TJU, International Campus of Tianjin University, Fuzhou 350207, China*

† Electronic supplementary information (ESI) available. See DOI: 10.1039/d1ta00012h

‡ These authors contributed equally to this work.

Herein, we report a molecular engineered Pd single atom catalyst with a pre-defined M-N_3C_1 coordination (Pd-N_3C_1-SAC), which shows a higher efficiency compared with SACs using the Pd-N_4 coordination. The as-synthesized SAC exists in the form of two-dimensional nanosheets, which allows them to be recovered readily from the reaction mixture and recycled. Owing to the enhanced electron density at the Pd centre, the Pd-N_3C_1-SAC was found to exhibit a lower reaction barrier (~0.31 eV difference) for Suzuki coupling. Utility was demonstrated by functionalization of indomethacin to afford derivatives in a late-stage setting. Such a strategy is universal and can be extended to Ni, Cu, and Sn-based systems.

Results and discussion

As shown in Fig. 1, our Pd SACs were synthesized by the pyrolysis of the corresponding Pd precursor (Pd-modified tetraphenylporphyrin, Pd-TPP for the Pd-N_4-SAC; and Pd-modified N-confused tetraphenylporphyrin, Pd-NCTPP[25–27] for the Pd-N_3C_1-SAC) and glutamic acid on an MgO template at 600 °C under Ar. After removing the template by acid wash, ultrathin Pd SACs with a typical thickness of ~2.5 nm were isolated as shown in the AFM images in Fig. 2c & S7.† FT-IR spectra of Pd SACs exhibited the strong C═N skeleton vibration from the porphyrin structure at 1400 cm^{-1} together with weak N–H and C–H vibrations. Such ultrathin morphology maximized the exposure of surface active sites to reactants owing to shortened diffusion pathways.[28,29] Our Pd SACs were also microporous, showing ultrahigh surface areas of 1025 and 832 m^2 g^{-1} from BET measurements of the Pd-N_3C_1-SAC and Pd-N_4-SAC with typical pore sizes of 0.5 and 1.4 nm, respectively. Detailed characterization of the chemical composition of precursors and SACs by UV-Vis, NMR, Raman, and FT-IR can be found in the ESI.†

We first characterized the atomic dispersion of Pd by scanning transmission electron microscopy in the annular dark field mode (STEM-ADF). The as-synthesized Pd SACs exhibited a two-dimensional nanosheet morphology (Fig. 2a). The replacement of TPP by NCTPP did not affect the dispersion of Pd atoms owing to abundant N ligands in the conjugated structure of porphyrin, whose uniform distribution was observed as bright spots as shown in Fig. 2b and c.[8] This was confirmed by the absence of Pd (111) and (200) peaks at ~40 and 45° in the XRD spectra. The Pd mass loading was determined to be 3.3% for the Pd-N_3C_1-SAC by inductively coupled plasma (ICP) analysis shown in Table S1.† The existence of Pd single atoms was further supported by energy-dispersive X-ray spectroscopy (EDS) elemental mapping in Fig. 2g and additional images in Fig. S8–S13.†[6]

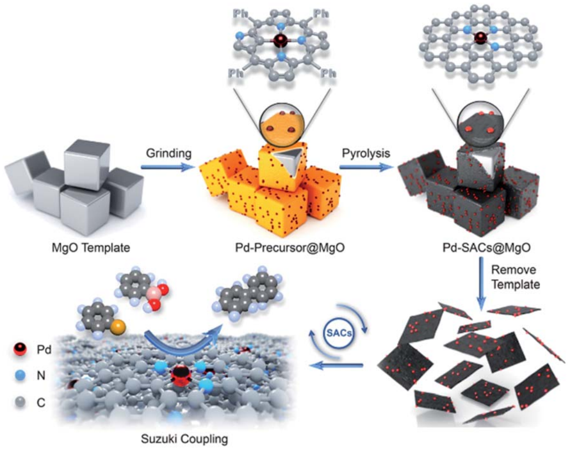

Fig. 1 Preparation of two-dimensional Pd SAC nanosheets with a precise M-N_3C_1 subunit for Suzuki coupling.

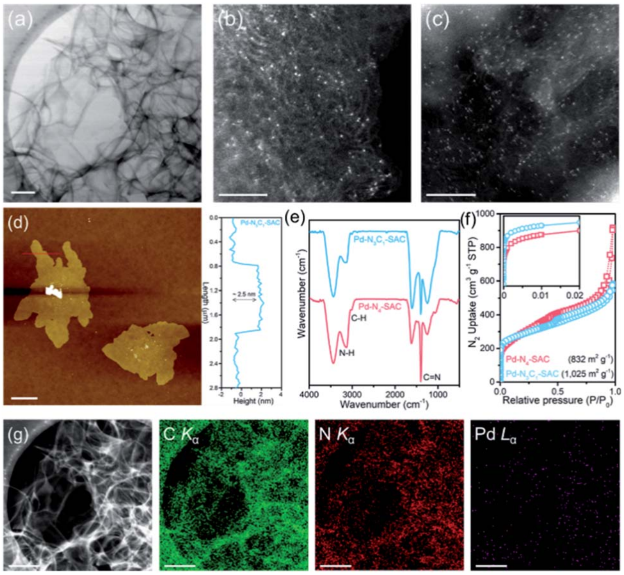

Fig. 2 Characterization of Pd SACs. (a, b) General view and atomic-resolution STEM-HAADF images for the Pd-N_3C_1-SAC and (c) Pd-N_4-SAC; (d) AFM topography and the corresponding line profile of the Pd-N_3C_1-SAC; (e) FT-IR spectra of Pd SACs showing a C═N rich backbone; (f) N_2 adsorption/desorption isotherms at 77 K; and (g) STEM EDS mapping of the Pd-N_3C_1-SAC. Scale bar: (a) 200 nm; (b, c) 5 nm; (d) 2 μm, (g) 200 nm.

The substitution by Pd–carbon bonds in the N-confused porphyrin and Pd-N_3C_1-SAC has a profound influence on the electronic structure.[25–27] The X-ray photoelectron spectra (XPS) of Pd_{3d} core-level displayed in Fig. 3a reveal that the characteristic peaks of Pd^{2+} $3d_{3/2}$ and $3d_{5/2}$ are negatively shifted to lower binding energies of 343.3 and 338.0 eV in the Pd-N_3C_1-SAC, respectively, indicating valence states that are between Pd^{1+} and Pd^{2+}, which are lower than that of the typical porphyrin-like structure.[15,25] The configuration of N in Pd SACs was also verified by N_{1s} core-level XPS spectra shown in Fig. 3b, in which pyrrolic N at 400.6 eV from N-confused porphyrin and pyridinic N at 398.9 eV from the pyrolysis of glutamic acid were dominant.[8,15] X-ray absorption spectroscopy (XAS) is a powerful technique to distinguish the electronic and coordination structure of SACs.[1] As shown in Fig. 3c, the extended X-ray absorption fine structure (EXAFS) spectra of Pd SACs exhibit a characteristic Pd–N peak at 1.4 Å that originates from the porphyrin precursors. This is distinct from the metallic Pd–Pd peak at 2.5 Å in Pd foil, suggesting the atomic dispersion of Pd

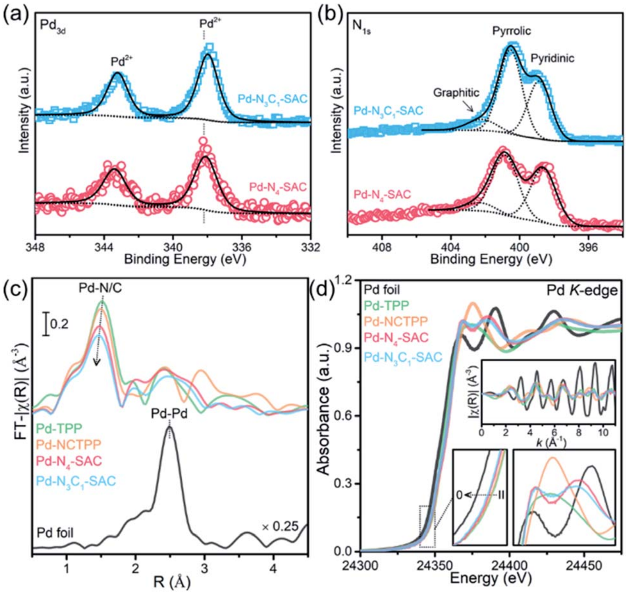

Fig. 3 Structural characterization of Pd SACs. (a) High-resolution XPS Pd_{3d} and (b) N_{1s} spectra of Pd SACs; (c) Pd *K*-edge FT-EXAFS spectra of Pd foil, Pd precursors and Pd SACs; (d) XANES spectra with enlarged images of the edge structure and white-line. The inset shows the corresponding EXAFS spectra.

in our catalysts.[8] The intensity of the Pd–N shell gradually decreases from Pd–TPP (precursor of the Pd-N_4-SAC) to the Pd-N_3C_1-SAC, as a result of the breakage of structural symmetry by carbon substitution and disturbance of the planar aromatic structure in the porphyrin scaffold after pyrolysis. Further analysis by EXAFS fitting shown in Fig. S14 and Table S2† confirmed a slightly lower coordination number of ~3 in the Pd-N_3C_1-SAC. Meanwhile, the oxidation state of Pd in the Pd-N_3C_1-SAC is estimated from the Pd K-edge X-ray absorption near edge structure (XANES) spectra shown in Fig. 3d, in which a slightly lower oxidation state (<+2) compared with porphyrin precursors and the unmodified Pd-N_4-SAC is revealed in the edge structure and white-line intensity; the oxidation state has also been confirmed from XANES simulation results shown in Fig. S15.†[23] Currently, most of the coordination structures were deduced from EXAFS fitting or calculations.[22–24] Pd SACs constructed from a molecularly precise precursor provide a well-defined environment for studying the dynamics of the metal–ligand coordination during the course of the reaction.[8]

We began with a standard Suzuki coupling reaction using iodobenzene and 4-methylphenylboronic acid with 1 mol% Pd catalyst, as shown in Fig. S16.† Both Pd SACs exhibited nearly quantitative conversion to the desired product, which was comparable to homogeneous catalysts $Pd(PPh_3)_4$ in terms of turnover frequency (TOF = 4.2 h^{-1}), and outperformed 10% Pd/C and $Pd(PPh_3)_2Cl_2$. Our Pd SACs displayed good cycling stability without any performance decay after 5 cycles. To demonstrate synthetic utility, a wide range of substrates were examined including those that are problematic using homogeneous catalysts,[8–11] including electron-rich and electron-deficient units on the aryl ring (–OMe, –CF_3, –NO_2 and acetyl), chemoselective Suzuki coupling of C–I bonds and heterocyclic substrates (benzodioxole, pyridines and thiophene that may poison the Pd catalyst by the coordination with N or S atoms) (Fig. S16†). For the 1,3,5-triiodobenzene substrate, the corresponding 1,3,5-triphenylbenzene was produced in quantitative yield. Notably, 9-cyanophenanthrene with potential utility in medicines can be generated in a one-pot reaction involving tandem Suzuki coupling and cyclization.[30]

Further catalyst screening was conducted using the less activated bromobenzene (Fig. 4), where conventional heterogeneous catalysts such as 10% Pd/C showed an inferior performance compared with the homogeneous catalyst $Pd(PPh_3)_4$ (8 *vs.* 94%). Notably, our Pd-N_3C_1-SAC exhibited a highly competitive yield (~90%) comparable to $Pd(PPh_3)_4$, and outperformed the Pd-N_4-SAC (10% yield). This could be attributed to the lower valence state and greater electron density of the Pd-N_3C_1-SAC.[23] The catalytic activity was strongly temperature dependent judging from the plot of yield *versus* temperature in Fig. 4b. Increasing the temperature from 90 to 110 °C increased the catalytic yield of the Pd-N_3C_1-SAC from 10% to 90%. A further increase to 120 °C resulted in a lower yield (75%) as a result of undesired homocoupling of boronic acids. Compared to the seminal research by Pérez-Ramírez *et al.*,[8] our Pd-N_3C_1-SAC has a higher TOF value upon completion of the reaction (3.8 *vs.* 1.9 h^{-1}, batch mode) and is easier to prepare than related homogeneous or supported porphyrin catalysts.[34,35]

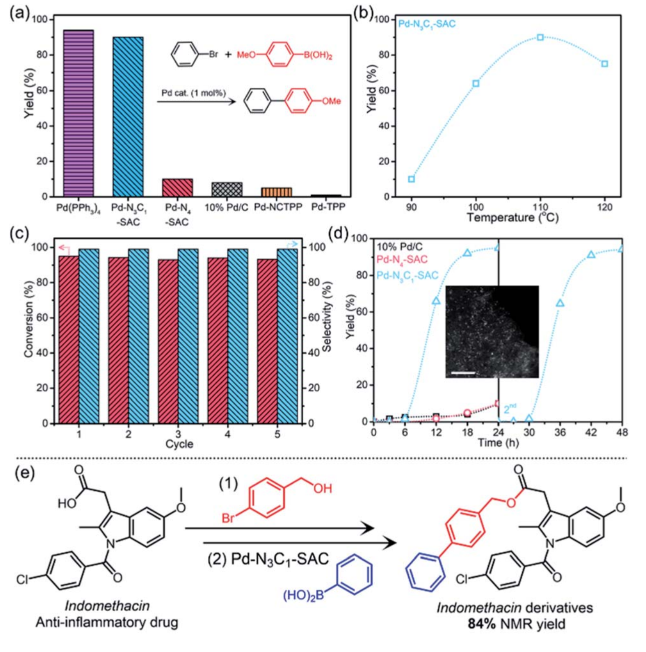

Fig. 4 Pd SAC-catalysed Suzuki coupling using bromo-compounds. (a) Catalyst screening. The inset shows the model reaction using 1 mol% Pd catalyst and 3 equiv. of K_2CO_3 in DME at 110 °C for 24 h; (b) temperature dependence on catalytic performance; (c) cycling stability and (d) kinetic study of the Pd-N_3C_1-SAC toward Suzuki coupling. The inset shows the representative STEM image of the spent catalyst; (e) demonstration of functional group compatibility in the synthesis of indomethacin derivatives using the Pd-N_3C_1-SAC. Scale bar: 5 nm.

Our study shows that SACs coordinated in a N-confused structure are powerful catalysts.[36,37]

Kinetic studies were conducted to provide insights into the reaction mechanism (Fig. 4d). We found that the Pd-N_3C_1-SAC was a superior catalyst to the Pd-N_4-SAC and Pd/C in view of its much faster reaction rate. A short induction period (∼6 h) was observed due to the complicated pathway (dynamic valence state changes of Pd SACs) to produce the coupling product. Further verification by hot-filtration experiments ruled out the possibility of the dissolution of the Pd SAC into homogeneous species.[8–11] No catalyst leaching into the supernatant of the reaction mixture was observed by ICP-OES. This was confirmed by the stability measurements shown in Fig. 4c, where our Pd-N_3C_1-SAC exhibited excellent catalytic performance for bromobenzene without significant decay after 5 cycles. The additional STEM image in the inset of Fig. 4d validated the atomic dispersion of the spent catalyst. The two-dimensional nanosheet structure of the Pd-N_3C_1-SAC maximizes the surface area for the reaction and its micron-size lateral dimension allows the catalyst to be separated from the reaction medium readily by filtration, unlike more tedious separation needed for homogeneous catalysts. Finally, to highlight the exceptional functional group compatibility, we had successfully transformed a substrate derived from multifunctional indomethacin, an FDA-approved anti-inflammatory drug, to its long-chain aromatic ester derivative in 84% NMR yield through sequential esterification and Suzuki coupling in the presence of the Pd-N_3C_1-SAC (Fig. 4e). This validates the usefulness of heterogeneous single atom catalysts for the production of high-value chemicals.

Our molecular engineering method can also be used to fabricate Ni, Cu, and Sn-based SACs (Fig. S19†), these are more sustainable alternative to Pd-based catalysts.[31–33,38] We have examined the use of nonprecious Ni-based SACs in Suzuki coupling, which has not been reported to date. As shown in Fig. S19,† by using the Ni-N_4-SAC and iodobenzene, ∼78% of the desired product can be obtained after preliminary optimizations. However, lower yields (60–32%) were observed for substrates containing electron-withdrawing groups. The Ni-N_3C_1-SAC also gave an unsatisfactory yield of 24% for the model reaction. Although further catalyst design is necessary to improve the catalytic efficiency, our work demonstrates the viability of metal-derived SACs in promoting important C–C bond forming transformations.

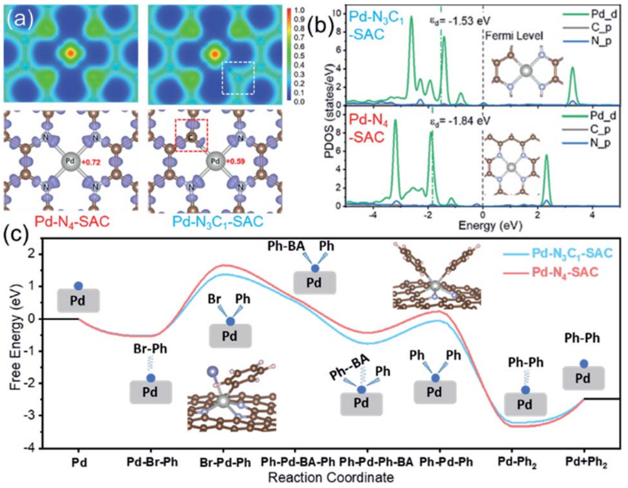

Fig. 5 DFT calculations of the reaction pathway. (a) Charge densities of the Pd-N_4-SAC and Pd-N_3C_1-SAC; (b) projected density of states (PDOS) for Pd, N and C for Pd SACs; (c) energy diagram and reaction pathways for the phosphine-free Suzuki coupling reaction between bromobenzene and phenylboronic acid in the presence of Pd SACs. Base and outer carbon atoms in the model are omitted for the sake for clarity. Color scheme used: brown for C, light blue for N, grey for Pd, blue for Br and light-pink for H.

Density functional theory (DFT) calculations were carried out to investigate the effect of changing from a N_4 to N_3C_1 coordination environment on the Suzuki coupling.[39–41] In Fig. 5a, the charge density of the Pd-N_4-SAC and Pd-N_3C_1-SAC were analyzed to identify the valence state of the Pd atom. Due to the different electron withdrawing properties of carbon, the Bader charge of Pd in the Pd-N_3C_1-SAC is lower than that of the Pd-N_4-SAC (+0.59 *vs.* +0.72), which reflects its lower oxidation state. Moreover, the projected density of states (PDOS) for the metal center and its coordinated N atoms were calculated to reveal the differences in the electronic structure of the active site. As shown in Fig. 5b, compared to the Pd-N_4-SAC, the d band of the Pd-N_3C_1-SAC is nearer to the Fermi level, which is indicative of higher reactivity. This is in accordance with a lower bandgap (−1.54 eV) and a lower valence state in XPS. The free energy diagrams of Suzuki coupling in Fig. 5c, S20 & S21† (base is omitted for the sake for clarity) reveal a similar adsorption barrier for the Pd-N_4-SAC and the Pd-N_3C_1-SAC at the beginning of the reaction, while subsequent activation of bromobenzene occurs with a much higher barrier for both and is rate-determining.[8] The reaction barrier for the Pd-N_3C_1-SAC is significantly lower than that of the Pd-N_4-SAC (0.31 eV difference) owing to its lower valence state and enhanced electron density on the Pd center to facilitate oxidative addition.[39–41] This was also reflected in the facile nucleophilic attack of the oxidation addition intermediate to phenylboronic acid, showing a more exothermic process on the surface of the Pd-N_3C_1-SAC than the Pd-N_4-SAC. Subsequent transmetalation of boronic acid with the assistance of the base is endothermic, where the Pd-N_3C_1-SAC also exhibits a diminished energy barrier. Finally, the C-C bond is formed after reductive elimination, delivering the desired product and regenerating the catalyst.[39–41] Based on the above DFT calculations, we conclude that the lower reaction barriers associated with the Pd-N_3C_1-SAC-catalysed sequence likely translate to better catalytic performance in the cross-coupling of bromobenzene.

Conclusions

In conclusion, the molecular engineering of two-dimensional Pd SACs using porphyrin precursors produced a unique M-N_3C_1 coordination in the Pd single atom, which led to a significant improvement in the efficiency of SAC-catalysed Suzuki coupling. The two-dimensional nanosheet structure of Pd-N_3C_1-SACs maximizes the surface area for the reaction and they can be readily separated from the reaction medium by filtration. The ability to control the hybridization of the single atom in a molecularly precise manner allows the catalytic mechanism to be studied in a well-defined manner; this paves the way forward to make more potent and atom-economic catalysts.

Author contributions

J. L. conceived the research, synthesized the materials, conducted catalytic reactions, and wrote the draft with K.·P. L., Z. C. and C. L. TEM, STEM characterization, and data analysis were conducted by J. L., and Z. C.; S. X., Y. D. and L. M. performed the EXAFS and data processing; W. Y. and X. Z. performed the XPS and Raman measurements; J. S. and X. S. performed the FTIR and XRD measurements. B. Z. and L. M. assisted in DFT calculations. C. L., and R. L. assisted with materials characterization and data analysis. M. J. K. and K.·P. L. supervised the research. All authors discussed and commented on the manuscript.

Conflicts of interest

There are no conflicts to declare.

Acknowledgements

J. L., Z. C. and C. L. contributed equally to this work. K. P. L. acknowledges NRF-CRP grant "Two-dimensional Covalent Organic Framework: Synthesis and Applications". Grant number NRF-CRP16-2015-02, funded by National Research Foundation, Prime Minister's Office, Singapore. M. J. K. thanks the National University of Singapore Academic Research Fund Tier 1: R-143-000-A77-114. L. M. thanks the financial support from National Natural Science Foundation of China (51302097 and 51571096). J. L. was supported by the Chinese Scholarship Council (CSC). This research used 7 of the National Synchrotron Light Source II, a U.S. Department of Energy (DOE) Office of Science User Facility operated for the DOE Office of Science by Brookhaven National Laboratory under Contract No. DE-SC0012704.

References

1 S. Ding, M. J. Hülesy, J. Pérez-Ramírez and N. Yan, *Joule*, 2019, **3**, 1–33.

2 A. Wang, J. Li and T. Zhang, *Nat. Rev. Chem.*, 2018, **2**, 65–81.

3 L. Liu and A. Corma, *Chem. Rev.*, 2018, **118**, 4981–5079.

4 L. Zhang, Y. Ren, W. Liu, A. Wang and T. Zhang, *Natl. Sci. Rev.*, 2018, **5**, 653–672.

5 H. Yan, C. Su, J. He and W. Chen, *J. Mater. Chem. A*, 2018, **6**, 8793–8814.

6 C. Liu, Z. Chen, H. Yan, S. Xi, K. M. Yam, J. Gao, Y. Du, J. Li, X. Zhao, K. Xie, H. Xu, X. Li, K. Leng, S. J. Pennycook, B. Liu, C. Zhang, M. J. Koh and K. P. Loh, *Sci. Adv.*, 2019, **5**, eaay1537.

7 Z. Chen, C. Liu, J. Liu, J. Li, S. Xi, X. Chi, H. Xu, I.-H. Park, X. Peng, X. Li, W. Yu, X. Liu, L. Zhong, K. Leng, W. Huang, M. J. Koh and K. P. Loh, *Adv. Mater.*, 2020, **32**, 1906437.

8 Z. Chen, E. Vorobyeva, S. Mitchell, E. Fako, M. A. Ortuño, N. López, S. M. Collins, P. A. Midgley, S. Richard, G. Vilé and J. Pérez-Ramírez, *Nat. Nanotechnol.*, 2018, **13**, 702.

9 E. Fernandéz, M. A. Rivero-Crespo, I. Domínguez, P. Rubio-Marqués, J. Oliver-Meseguer, L. Liu, M. Cabrero-Antonino, R. Gavara, J. C. Hernández-Garrido, M. Boronat, A. Leyva-Pérez and A. Corma, *J. Am. Chem. Soc.*, 2019, **141**, 1928–1940.

10 G. Ding, L. Hao, H. Xu, L. Wang, J. Chen, T. Li, X. Tu and Q. Zhang, *Commun. Chem.*, 2020, **3**, 43.

11 E.-K. Lee, S.-A. Park, H. Woo, K. H. Park, D. W. Kang, H. Lim and Y.-T. Kim, *J. Catal.*, 2017, **352**, 388–393.

12 X. Zhang, Z. Sun, B. Wang, Y. Tang, L. Nguyen, Y. Li and F. F. Tao, *J. Am. Chem. Soc.*, 2018, **140**, 954–962.

13 L. Zhang, A. Wang, J. T. Miller, X. Liu, X. Yang, W. Wang, L. Li, Y. Huang, C.-Y. Mou and T. Zhang, *ACS Catal.*, 2014, **4**, 1546–1553.

14 J. Zhang, X. Wu, W.-C. Cheong, W. Chen, R. Lin, J. Li, L. Zheng, W. Yan, L. Gu, C. Chen, Q. Peng, D. Wang and Y. Li, *Nat. Commun.*, 2018, **9**, 1002.

15 H. Yan, H. Cheng, H. Yi, Y. Lin, T. Yao, C. Wang, J. Li, S. Wei and J. Lu, *J. Am. Chem. Soc.*, 2015, **137**, 10484–10487.

16 S. Zhou, L. Shang, Y. Zhao, R. Shi, G. I. N. Waterhouse, Y.-C. Huang, L. Zheng and T. Zhang, *Adv. Mater.*, 2019, **31**, 1900509.

17 S. Wei, A. Li, J.-C. Liu, Z. Li, W. Chen, Y. Gong, Q. Zhang, W.-C. Cheong, Y. Wang, L. Zheng, H. Xiao, C. Chen, D. Wang, Q. Peng, L. Gu, X. Han, J. Li and Y. Li, *Nat. Nanotechnol.*, 2018, **13**, 856–861.

18 Q. Zuo, T. Liu, C. Chen, Y. Ji, X. Gong, Y. Mai and Y. Zhou, *Angew. Chem., Int. Ed.*, 2019, **58**, 10198–10203.

19 Y. Zhao, H. Zhou, W. Chen, Y. Tong, C. Zhao, Y. Lin, Z. Jiang, Q. Zhang, Z. Xue, W.-C. Cheong, B. Jin, F. Zhou, W. Wang, M. Chen, X. Hong, J. Dong, S. Wei, Y. Li and Y. Wu, *J. Am. Chem. Soc.*, 2019, **141**, 10590–10594.

20 J. Li, L. Zhong, L. Tong, Y. Yu, Q. Liu, S. Zhang, C. Yin, L. Qiao, S. Li, R. Si and J. Zhang, *Adv. Funct. Mater.*, 2019, **29**, 1905423.

21 X. He, Q. He, Y. Deng, M. Peng, H. Chen, Y. Zhang, S. Yao, M. Zhang, D. Xiao, D. Ma, B. Ge and H. Ji, *Nat. Commun.*, 2019, **10**, 3663.

22 X. Wang, Z. Chen, X. Zhao, T. Yao, W. Chen, R. You, C. Zhao, G. Wu, J. Wang, W. Huang, J. Yang, X. Hong, S. Wei, Y. Wu and Y. Li, *Angew. Chem., Int. Ed.*, 2018, **57**, 1944–1948.

23 Y. Pan, Y. Chen, K. Wu, Z. Chen, S. Liu, X. Cao, W.-C. Cheong, T. Meng, J. Luo, L. Zheng, C. Liu, D. Wang, Q. Peng, J. Li and C. Chen, *Nat. Commun.*, 2019, **10**, 4290.

24 Y.-N. Gong, L. Jiao, Y. Qian, C.-Y. Pan, L. Zheng, X. Cai, B. Liu, S.-H. Yu and H.-L. Jiang, *Angew. Chem., Int. Ed.*, 2020, **59**, 2705–2709.

25 J. D. Harvey and C. J. Ziegler, *Coor. Chem. Rev.*, 2003, **247**, 1–19.

26 H. Furuta, T. Asano and T. Ogawa, *J. Am. Chem. Soc.*, 1994, **116**, 767–768.

27 H. Furuta, H. Maeda and A. Osuka, *J. Am. Chem. Soc.*, 2000, **122**, 803–807.

28 J. Deng, H. Li, J. Xiao, Y. Tu, D. Deng, H. Yang, H. Tian, J. Li, P. Ren and X. Bao, *Energy Environ. Sci.*, 2015, **8**, 1594.

29 Y. Zhu, W. Sun, J. Luo, W. Chen, T. Cao, L. Zheng, J. Dong, J. Zhang, M. Zhang, Y. Han, C. Chen, Q. Peng, D. Wang and Y. Li, *Nat. Commun.*, 2018, **9**, 3861.

30 Y. H. Kim, H. Lee, Y. J. Kim, B. T. Kim and J. N. Heo, *J. Org. Chem.*, 2008, **73**, 495–501.

31 J. A. Widegren and R. G. Finke, *J. Mol. Catal. A Chem.*, 2003, **198**, 317–341.

32 N. T. S. Phan, M. Van Der Sluys and C. W. Jones, *Adv. Synth. Catal.*, 2006, **348**, 609–679.

33 S. Z. Tasker, E. A. Standley and T. F. Jamison, *Nature*, 2014, **509**, 299–309.

34 K. U. Rao, R. M. Appa, J. Lakshmidevi, R. Vijitha, K. S. V. K. Rao, M. Narasimhulu and K. Venkateswarlu, *Asian J. Org. Chem.*, 2017, **6**, 751–757.

35 P. Ju, S. Wu, Q. Su, X. Li, Z. Liu, G. Li and Q. Wu, *J. Mater. Chem. A*, 2019, **7**, 2660–2666.

36 T. Miyazaki, T. Yamamoto, S. Mashita, Y. Deguchi, K. Fukuyama, M. Ishida, S. Mori and H. Furuta, *Eur. J. Inorg. Chem.*, 2018, **22**, 203–207.

37 J. B. dela Cruz, M. Ruamps, S. Arco and C.-H. Hung, *Dalton Trans.*, 2019, **48**, 7527–7531.

38 J. E. Zweig, D. E. Kim and T. R. Newhouse, *Chem. Rev.*, 2017, **117**, 11680–11752.

39 Z. Chen, E. Vorobyeva, S. Mitchell, E. Fako, N. López, S. M. Collins, R. K. Leary, P. A. Midgley, R. Hauert and J. Pérez-Ramírez, *Natl. Sci. Rev.*, 2018, **5**, 642–652.

40 Q. Feng, S. Zhao, Y. Wang, J. Dong, W. Chen, D. He, D. Wang, J. Yang, Y. Zhu, H. Zhu, L. Gu, Z. Li, Y. Liu, R. Yu, J. Li and Y. Li, *J. Am. Chem. Soc.*, 2017, **139**, 7294–7301.

41 L. Xue and Z. Lin, *Chem. Soc. Rev.*, 2010, **39**, 1692–1705.